Dichotomously switched phase flows

Simon J. Fraser and Raymond Kapral
Chemical Physics Theory Group, Department of Chemistry, University of Toronto, Toronto, Ontario, Canada M5S 3H6
(Received 5 May 1997)

The general formalism for periodic dichotomous noise on nonpotential flows is considered. This uncorrelated noise process switches suddenly at integer values of period τ. The effect of additive noise of this kind on the planar FitzHugh-Nagumo ordinary differential equations [R. FitzHugh, Biophys. J. **1**, 445 (1961); J. Nagumo, S. Arimoto, and Y. Yoshikawa, Proc. IRE **50**, 2061 (1962)] is examined. For large τ, quasifractal attractors are observed, whereas for the white-noise limit, where τ is small, a Fokker-Planck equation describes the evolution. The magnitude of τ determines the smoothness of the transient evolution and equilibrium density of the system. Typically the stochastic equations give rise to two regions of high density near the stable fixed points of the underlying autonomous system. The stiffness parameter ε in the differential equations determines the fast variable, its associated nullcline, and the resulting flow structure. For small ε the cubic nullcline controls the motion and transitions between the high-density peaks occur along segments of a noisy limit cycle. For large ε the linear nullcline governs the transitions and the peaks are joined by a single band. The statistical behavior of the oscillatory and direct transitions is examined. [S1063-651X(97)01209-9]

PACS number(s): 05.40.+j, 05.45.+b, 02.50.−r, 46.10.+z

I. INTRODUCTION

Nonlinear systems driven by colored noise have interesting structural and dynamical properties. The stationary distribution, if it exists, may have extrema different from those of the underlying deterministic system and the transition rates between regions of high probability depend in subtle ways on the correlations in the noise process that is responsible for the transitions. There exists an extensive literature on the calculation of transition rates in overdamped, one-dimensional systems governed by a quartic potential subject to various types of colored noise [1].

If the dissipative deterministic dynamics is two-dimensional and cannot be derived from a potential, limit-cycle oscillations as well as fixed-point attractors may exist. When such two-dimensional systems are driven by colored noise the resulting phase-space flow may be complicated but structured [2]. In addition, the new time scale associated with the oscillatory dynamics may be comparable to that of the noise correlation time and influence the transition rate process [3].

In this article we consider such effects for a specific but often studied two-dimensional system: the FitzHugh-Nagumo model [4]. While this model was originally introduced in the context of nerve impulse propagation, it has seen widespread use since it exhibits excitability, bistability, and oscillations and the structure of the ordinary differential equations describing its dynamics has features in common with many systems. The two variables in this model are often referred to as the activator and inhibitor and their relative velocities are determined by a control parameter ε.

We restrict our considerations to a specific simple colored-noise process: periodic dichotomous noise [5,6]. This noise process causes the system to switch between two alternative forms of the evolution equations with probabilities p and $q=1-p$ at regular time intervals τ [7]. In the studies presented here the two evolution equations are of FitzHugh-Nagumo type and differ in their additive or multiplicative control parameters; thus it may serve as a model for chemical systems with activator-inhibitor kinetics where the flow terms are stochastic variables. By selecting parameters in the stochastic process one may then study transitions between fixed points, a fixed point and limit cycle, or two limit cycles.

The outline of the paper is as follows. Section II describes the stochastic dynamics in general, formal terms without regard to a specific deterministic dynamics. Both stochastic differential equations and Fokker-Planck equations are presented for the periodic dichotomous noise process. In Sec. III the results are specialized to the FitzHugh-Nagumo model and the focus is placed on additive noise in both the slow- and fast-inhibitor limits. Passage to the white-noise limit is considered and the fast-inhibitor limit is treated in some detail where passage to this limit presents some subtle features. Section IV is devoted to the discussion of the noisy attractors as a function of the noise period τ and the FitzHugh-Nagumo variable ε. The change in attractor structure as the white-noise limit is approached is also discussed. Transition rate processes between stable states are described in Sec. V. We consider cases where the transition process gives rise to monotonic and oscillatory decay to the stationary distribution and examine the features responsible for this behavior. The conclusions of the study are given in Sec. VI.

II. EVOLUTION UNDER PERIODIC DICHOTOMOUS NOISE

Before turning to the stochastically driven FitzHugh-Nagumo (FHN) equation, which forms the central part of our study, it is useful to present a general formulation of the model that does not rely on the specific details of the FHN dynamics. Let $\mathbf{x}=(x_1,x_2,\ldots,x_n)$ be a vector of dynamical variables and $\mathbf{f}_{\pm}$ two (possibly nonlinear) functions of $\mathbf{x}$. We suppose that the time evolution of $\mathbf{x}(t)$ is given by the stochastic model

$$\dot{\mathbf{x}}(t)=\frac{1}{2}[1+\nu(t)]\mathbf{f}_+(\mathbf{x}(t))+\frac{1}{2}[1-\nu(t)]\mathbf{f}_-(\mathbf{x}(t)). \quad (1)$$

Here $\nu(t)$ is the continuous-time periodic dichotomous noise process

$$\nu(t)=\sum_{s=0}^{\infty}\nu_s\theta(t-s\tau)\theta((s+1)\tau-t), \quad t\geqslant 0, \quad (2)$$

driven by the discrete (Bernoulli trial) noise process ν_s, for $s\in\mathbb{Z}^+$, defined by

$$\nu_s=\begin{cases}+1, & \text{probability } p\\ -1, & \text{probability } q,\end{cases} \quad (3)$$

where $q=1-p$. In Eq. (2), θ is the Heaviside function.

The stochastic differential equation (1) can be integrated over the time interval τ to give the two-branched stochastic map

$$\mathbf{x}_\pm(t+\tau)=\int_t^{t+\tau}\mathbf{f}_\pm(\mathbf{x}(t'))dt'+\mathbf{x}(t)=e^{\mathcal{L}_\pm^\dagger\tau}\mathbf{x}(t)\equiv\mathbf{F}_\pm^\tau(\mathbf{x}(t)), \quad (4)$$

where $\mathcal{L}_\pm^\dagger(\mathbf{x})=\mathbf{f}_\pm(\mathbf{x})\cdot\nabla$. In Eq. (4), at instants $t=s\tau$, the positive branch is chosen with probability p and the negative branch is chosen with probability q. In this stroboscopic picture a stochastic trajectory is a sequence of points functionally dependent on an underlying sequence of Bernoulli trials.

The stochastic differential equation (1) is associated with a two-component Fokker-Planck equation for densities $\rho_\pm(\mathbf{x},t)$ controlled by velocity fields $\mathbf{f}_\pm$:

$$\begin{pmatrix}[\partial_t+\mathcal{L}_+(\mathbf{x})]\rho_+(\mathbf{x},t)\\ [\partial_t+\mathcal{L}_-(\mathbf{x})]\rho_-(\mathbf{x},t)\end{pmatrix}=\sum_{s=0}^{[t/\tau]}\delta(t-s\tau)\begin{pmatrix}-q & p\\ q & -p\end{pmatrix}\times\begin{pmatrix}\rho_+(\mathbf{x},t)\\ \rho_-(\mathbf{x},t)\end{pmatrix}, \quad (5)$$

where $\mathcal{L}_\pm(\mathbf{x})=\nabla\cdot\mathbf{f}_\pm(\mathbf{x})$ and $[t/\tau]$ is the largest integer less than t/τ. Each component in this equation can be integrated over the noise period τ and added to give a discrete evolution equation for the total density $\rho(\mathbf{x},t)=\rho_+(\mathbf{x},t)+\rho_-(\mathbf{x},t)$ [8]:

$$\rho(\mathbf{x},t+\tau)=(pe^{-\mathcal{L}_+\tau}+qe^{-\mathcal{L}_-\tau})\rho(\mathbf{x},t). \quad (6)$$

This equation induces a diffeomorphism of $\mathbb{R}^n$ into $\mathbb{R}^n$ when written as an integral equation with singular kernel over the spatial coordinates (Perron-Frobenius equation):

$$\rho(\mathbf{x},t+\tau)=\int d\mathbf{y}\{p\,\delta(\mathbf{x}-e^{\mathcal{L}_+^\dagger\tau}\mathbf{y})+q\,\delta(\mathbf{x}-e^{\mathcal{L}_-^\dagger\tau}\mathbf{y})\}\rho(\mathbf{y},t)$$
$$=\int d\mathbf{y}\{p\,\delta(\mathbf{x}-\mathbf{F}_+^\tau(\mathbf{y}))+q\,\delta(\mathbf{x}-\mathbf{F}_-^\tau(\mathbf{y}))\}\rho(\mathbf{y},t). \quad (7)$$

Here $\mathbf{F}_\pm^\tau(\mathbf{x})=\exp(\mathcal{L}_\pm^\dagger\tau)\mathbf{x}$ are just the two map branches (4) appearing in the integrated (stroboscopic) form of the stochastic differential equation (1).

A question that arises in the case of the singular integral equation (7) is whether the asymptotic state possesses an invariant density $\rho^*(\mathbf{x})\equiv\lim_{t\to\infty}\rho(\mathbf{x},t)$. The symmetric Bernoulli convolution on the unit interval that can be written in the form of Eq. (7) is an important example where ρ^* does not exist when the mass of the system is eventually concentrated on a (dense or nowhere dense) set of measure zero [9,10]. However, we avoid the problem of the existence of ρ^* by coarse graining. A coarse-grained density defined as the mean probability of the measure in a lattice partition of (phase) space always exists.

III. FITZHUGH-NAGUMO EQUATION: STOCHASTIC DYNAMICS

As an example of a two-dimensional flow consider the FitzHugh-Nagumo equation [4]

$$\frac{du}{dt}=u-u^3-v, \quad \frac{dv}{dt}=\varepsilon(u-\alpha v-\beta), \quad (8)$$

or

$$\dot{\mathbf{x}}(t)=\mathbf{f}(\mathbf{x}(t);\alpha,\beta), \quad (9)$$

where we have set $\mathbf{x}=(u,v)^T$ and $\mathbf{f}$ is defined by the right-hand sides of Eq. (8). This equation possesses cubic and linear nullclines that may intersect to produce a variety of different attractors. We may convert this into a stochastic differential equation with two kinds of periodic dichotomous noise: α fluctuation leads to multiplicative noise and β fluctuation leads to additive noise; we focus here on the additive-noise case. We now examine the structure of the autonomous vector fields corresponding to the components of the random variables and their averages.

Suppose α is fixed and the random variable $\beta(t)$ takes the two values $\pm\Delta$ with probabilities p and q, respectively, at integer multiples of τ. The stochastic differential equation now takes the form of Eq. (1) with

$$\mathbf{f}_\pm(\mathbf{x}(t))=\begin{pmatrix}u-u^3-v\\ \varepsilon(u-\alpha v\mp\Delta)\end{pmatrix}. \quad (10)$$

Consider the situation shown in Fig. 1. The heavy solid lines are the two nullclines for $\beta=0$ that intersect in three fixed points, two of which are stable (large filled circles) and the other (open circle) unstable. If $\beta(t)$ takes the values $\pm\Delta$ the linear nullcline is replaced by two new linear nullclines (dashed lines). Depending on the amplitude Δ and the parameter α, each of these linear nullclines may intersect the cubic nullcline in one, two, or three fixed points. For sufficiently small Δ there are three fixed points on each branch and the outer two will remain stable as Δ increases. The noise process will involve random motion of the phase point about the stable fixed points; once the phase point lies in the vicinity of a fixed point it will never leave this region. As Δ increases a pair of fixed points on either branch coalesces. As Δ increases further there is only one intersection of the nullclines for each branch. This situation is depicted as dashed lines in Fig. 1, each of which now intersects the cubic nullcline in a single stable fixed point (small filled circles).

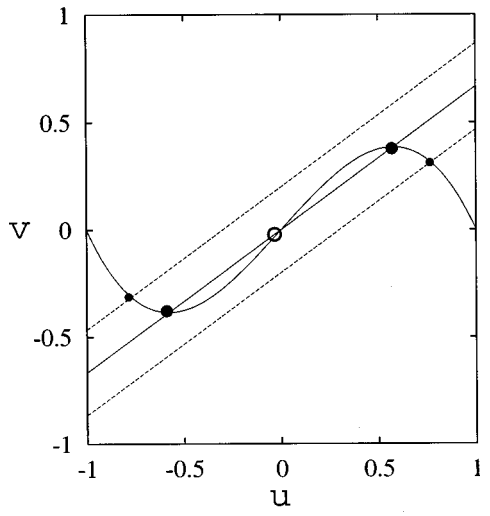

FIG. 1. Nullclines for the FHN model. $\alpha=1.5$ and $\beta=0$. The dashed linear nullclines correspond to $\pm\Delta=\pm 0.3$.

Periodic dichotomous switching then leads to noise-induced transitions between these two fixed points.

In Eq. (8), ε is a stiffness parameter. For ε very large, v, the inhibitor, is the fast variable and the linear nullcline dominates the motion whereas for ε very small, v is the slow variable and the motion is controlled by the cubic nullcline. Since the outer branches of the cubic nullcline are stable and the inner branch is unstable the motion has the character of a relaxation oscillation.

A. White-noise limit

There are several possible parameter variations to consider in the FHN model in the parameter space $\varepsilon\times\tau\times\Delta$. One interesting case is the white-noise limit where we fix ε and move in the (τ,Δ) parameter plane such that $\Delta^2\tau$ remains fixed; then the white-noise limit is recovered as $\tau\to 0$ and $\Delta\to\infty$ for $\Delta^2\tau=D$.

The two-dimensional Fokker-Planck equation corresponding to the FHN model is then obtained by expanding the evolution operators in Eq. (6) to $O(\tau^2)$ and dividing by τ. Formally,

$$\frac{1}{\tau}[\rho(\mathbf{x},t+\tau)-\rho(\mathbf{x},t)] = \frac{1}{\tau}\left\{p\left[1-\mathcal{L}_+\tau+\frac{1}{2}(\mathcal{L}_+\tau)^2\right] + q\left[1-\mathcal{L}_-\tau+\frac{1}{2}(\mathcal{L}_-\tau)^2\right]-1\right\}\rho(\mathbf{x},t),$$

where the operators $\mathcal{L}_\pm=\nabla\cdot\mathbf{f}_\pm(\mathbf{x})$ act on everything to their right.

Explicitly evaluating the $O(\tau)$ and $O(\tau^2)$ terms gives

$$\partial_t\rho=-\{\partial_u(u-u^3-v)+\partial_v\varepsilon(u-\alpha v)+\partial_v\varepsilon\Delta(q-p)\}\rho + \frac{1}{2}\varepsilon^2 D\partial_{vv}\rho, \tag{11}$$

where we must take $p=q=\frac{1}{2}$ to remove the divergent velocity bias term; all other terms vanish as $\tau\to 0$. Diffusion occurs in the v direction with diffusion constant $\varepsilon^2 D$ because only this variable is subject to noise. Dispersion in the u direction is then the result of coupling through the drift term. This motion resembles the Ornstein-Uhlenbeck process [11].

B. Fast-inhibitor limit

We may consider the fast-inhibitor limit of the FHN model where $\varepsilon\to\infty$; v is entrained by u, i.e., $v=v(u)$, and Eq. (8) reduces to

$$\frac{du}{dt}=-u^3+(1-\alpha^{-1})u+\beta(t)/\alpha=-\frac{dV(u)}{du}+\beta(t)/\alpha, \tag{12}$$

where the potential $V(u)=u^4/4-(1-\alpha^{-1})u^2/2$. The one-variable stochastic differential equation may be integrated over the time interval τ to yield the stochastic map

$$u_\pm(t+\tau)=\begin{cases} C^\tau(u(t),+\Delta/\alpha), & \text{probability } p \\ C^\tau(u(t),-\Delta/\alpha), & \text{probability } q, \end{cases} \tag{13}$$

where the nonlinear function $C^\tau\equiv C^\tau_\pm$ may be determined implicitly from the integration of the cubic velocity field:

$$C^\tau(u(\tau),\pm\Delta/\alpha):\tau=-A^{-1}\sum_{j=1}^{3} a_j\frac{u(\tau)\pm u_j}{u(0)\pm u_j}, \tag{14}$$

where $A=\Sigma_{j=1}^{3}u_ju_{j+1}(u_j-u_{j+1})$ and $a_j=u_{j+1}-u_{j+2}$ with subscript addition mod 3. Here u_j is a root of $-u^3+u+\Delta/\alpha$. This one-dimensional cubic case was studied in some detail in Ref. [12]. One of the important organizing features is the existence of eventually periodic orbits in which transients from the fixed points reach a centrally periodic orbit in a finite number of steps [6,12]. The structure of the coarse-grained invariant density in the (u,τ) plane is determined by the images of the transients under the map branches; centrally periodic orbits correspond to branch crossings and are associated with singular measures.

As an example consider the period-2 eventually periodic orbit shown in Fig. 2. Using the conditions that the fixed points of the map branches map into the central period-2 orbit, we find that this orbit arises at $\tau=2.857\,413\,26$ for $\alpha=3/2$ and $\Delta=1/3$. The coarse-grained probability density shown in Fig. 3 is peaked near the period-2 fixed points and the map fixed points with gaps between these regions. In Fig. 4 we compare this coarse-grained density for the one-variable model with that for the full stochastic FHN equation projected onto the u variable for $\varepsilon=1$, a relatively large value. Again the density is strongly peaked near the period-2 points, but the fine structure is different. In both cases the existence of the underlying, eventually periodic period-2 orbit serves to organize the structure of the dynamics and the resulting coarse-grained probability density.

The white-noise limit of the stochastic differential equation (12) is described by the Fokker-Planck equation

$$\partial_t\rho=-\partial_u[-u^3+(1-\alpha^{-1})u]\rho+\frac{1}{2}\widetilde{D}\partial_{uu}\rho, \tag{15}$$

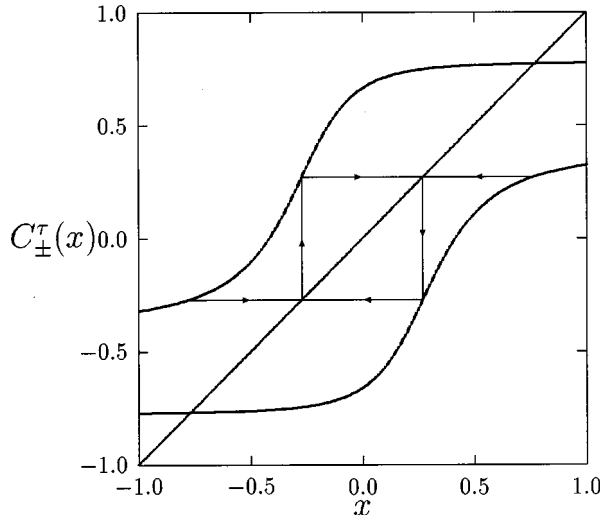

FIG. 2. Eventual period-2 orbit at $\alpha=3/2$, $\Delta=1/3$, and $\tau=2.857\,413\,26$.

where $\rho=\rho(u,t)$ and the diffusion coefficient $\widetilde{D}$ now takes the form $\widetilde{D}=D/\alpha^2$. The stationary density is

$$\rho^*(u)=Ne^{-2V(u)/\widetilde{D}}. \tag{16}$$

It is instructive to consider the white-noise and fast-inhibitor limits in more detail. Above, the one-variable Fokker-Planck equation (15) was derived from the one-variable stochastic differential equation (12), after the fast-inhibitor limit was taken. In contrast, the two-variable Fokker-Planck equation (11) cannot be directly reduced to the one-variable form as $\varepsilon\to\infty$ due to the fact that these two limits do not commute. It is possible to carry out a reduction of the two-variable Perron-Frobenius equation (7) to Eq. (15) by careful consideration of the fast-inhibitor and white-noise limiting processes. This derivation is carried out in the Appendix.

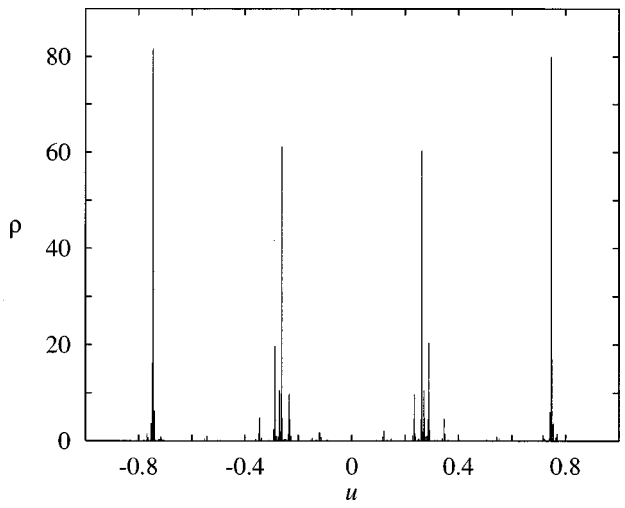

FIG. 3. Histogram of the density for the central period-2 orbit at $\alpha=3/2$, $\Delta=1/3$, and $\tau=2.857\,413\,26$ shown in Fig. 2.

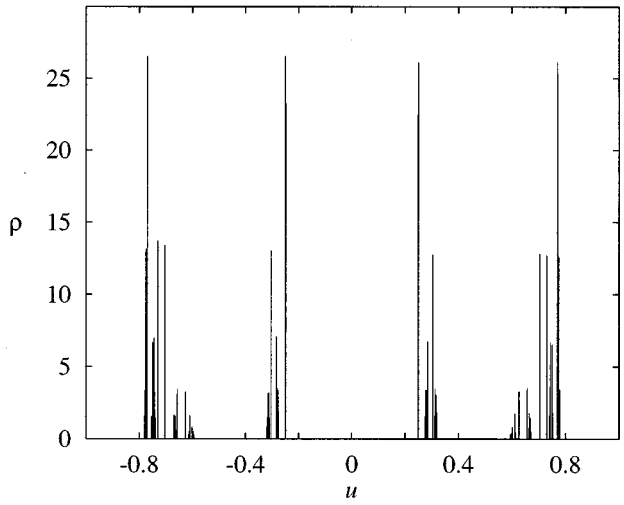

FIG. 4. Histogram of the phase-space density projected onto the u axis for FHN stochastic differential equations at parameters $\alpha=3/2$, $\Delta=0.3$, and $\tau=2.857\,413\,26$, corresponding to the central period-2 orbit in Fig. 2.

C. Slow-inhibitor limit

In order to investigate the slow-inhibitor limit $\varepsilon\to0$ it is convenient to consider the scaled time variables $t'=\varepsilon t$ and $\tau'=\varepsilon\tau$. In terms of these variables we may rewrite the FHN equations (8) as

$$\frac{du}{dt'}=\varepsilon^{-1}(u-u^3-v), \quad \frac{dv}{dt'}=u-\alpha v-\beta(t'). \tag{17}$$

In the slow inhibitor limit u is entrained by v, so we write

$$\frac{dv}{dt'}=u(v)-\alpha v-\beta(t'), \tag{18}$$

where $u(v)$ is obtained from the solutions of $u-u^3-v=0$. The S-shaped u nullcline has three branches when the system has three real roots. Consequently, in the slow-inhibitor limit the v variable executes stochastic dynamics on the two branches corresponding to the stable fixed points and makes discontinuous hops between them. These two branches are given by

$$u_1(v)=\frac{2}{\sqrt{3}}\cos\phi, \quad u_2(v)=\frac{1}{\sqrt{3}}\left[-\cos\frac{\phi}{3}-\sqrt{3}\sin\frac{\phi}{3}\right], \tag{19}$$

where $\phi=\cos^{-1}(-3\sqrt{3}v/2)$. Thus, in this slow-inhibitor limit the stochastic dynamics resembles that of a noisy relaxational limit cycle when plotted in the (u,v) plane, where motion on the two u nullclines is distinguished. Figure 5 shows the stable branches of the cubic nullclines given in Eq. (19) along with the unstable branch. The stochastic dynamics of the FHN model for a small value of ε ($\varepsilon=0.01$) is also shown in this figure. As predicted, the stochastic dynamics tracks the stable branches of the cubic nullcline with rapid, nearly vertical hops between them.

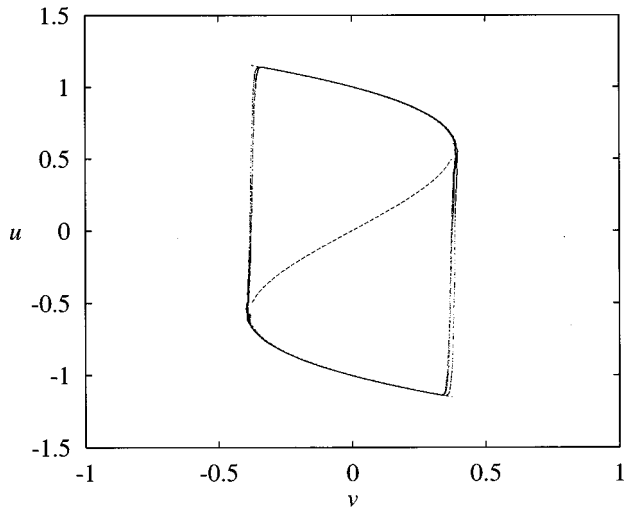

FIG. 5. Stable [Eq. 19] and unstable branches of the cubic nullcline and the limit-cycle-like trajectory for $\varepsilon=0.01$, $\alpha=1.45$, and $\Delta=1.4$.

IV. ATTRACTOR STRUCTURE

In this section we examine the structure of the attractors for various values of the parameters and also study how these attractors deform as the white-noise limit is approached.

A. Overview of attractor structure

Figure 6 shows the structure of the attractors in the (ε,τ) plane for $\Delta=0.3$ and $p=q=1/2$. Each attractor is displayed in the (u,v) plane and all attractors are drawn on the same scale with $-1.5\leqslant u\leqslant 1.5$ and $-0.6\leqslant v\leqslant 0.6$. The individual figures in this collection of attractors are labeled by their coordinates in the (ε,τ) plane. Note that for these parameters all attractors are centrosymmetric in accord with the symmetry properties of the equations.

We now examine the dynamics that generates the attractors in Fig. 6. First, we consider the fast-inhibitor regime where ε is large. In this case the trajectories remain close to the linear nullcline. The attractor structure also depends on τ and when τ is very small compared to any other time scale the representative point moves in the averaged vector field driven by high-frequency noise. As is seen in the lower left corner of Fig. 6, the high-frequency stochastic process leads to a bimodal structure.

As τ increases and becomes comparable to the intrinsic time scale of the underlying dynamics, persistence of trajectories or flow structure becomes apparent in the attractors. In Fig. 6 this is first evident as diagonal striations, which suggest the emergence of singular measures for the attractors. As τ increases further lacunae appear in the support of the attractors. Replicas of the foci and nullclines of the underlying autonomous vector field emerge. Because v is the fast variable the attractor becomes ''thin'' transverse to the v nullcline and remains linelike along this nullcline direction. When τ is larger than any intrinsic time scale these linelike structures break up into a dust, as seen in the upper left portion of the figure.

In the slow-inhibitor limit, when ε is small the trajectories remain close to the cubic u nullcline during the slow part of

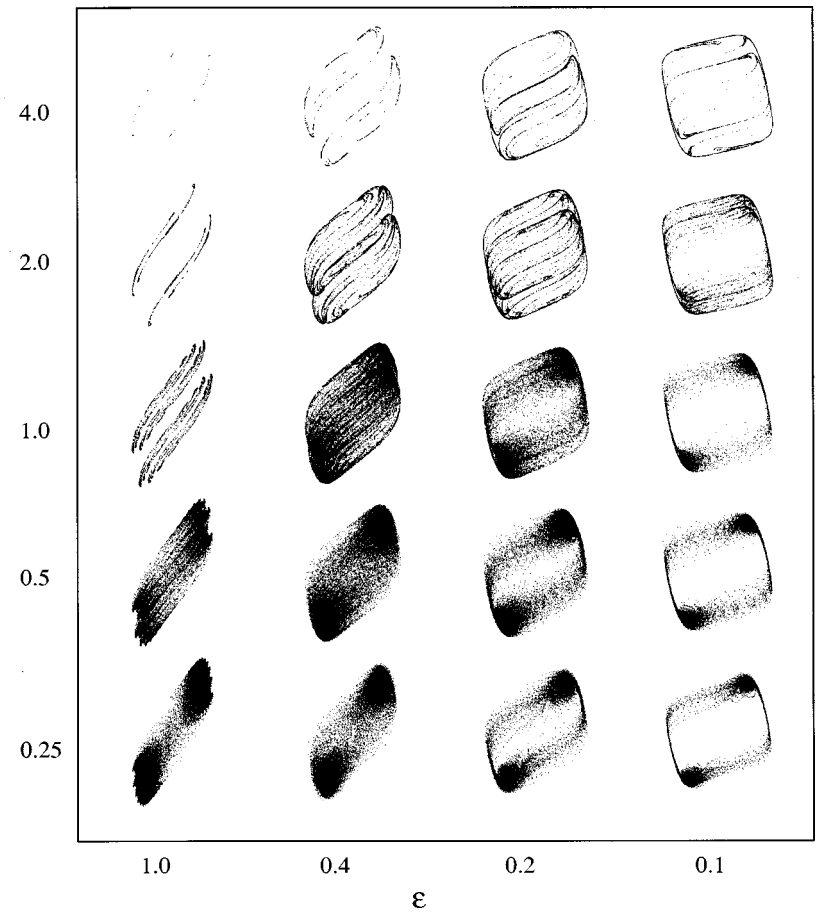

FIG. 6. Set of attractors for various values of ε (abscissa) and τ (ordinate). Each attractor portrait is a representation of the attractor in the (u,v) phase plane.

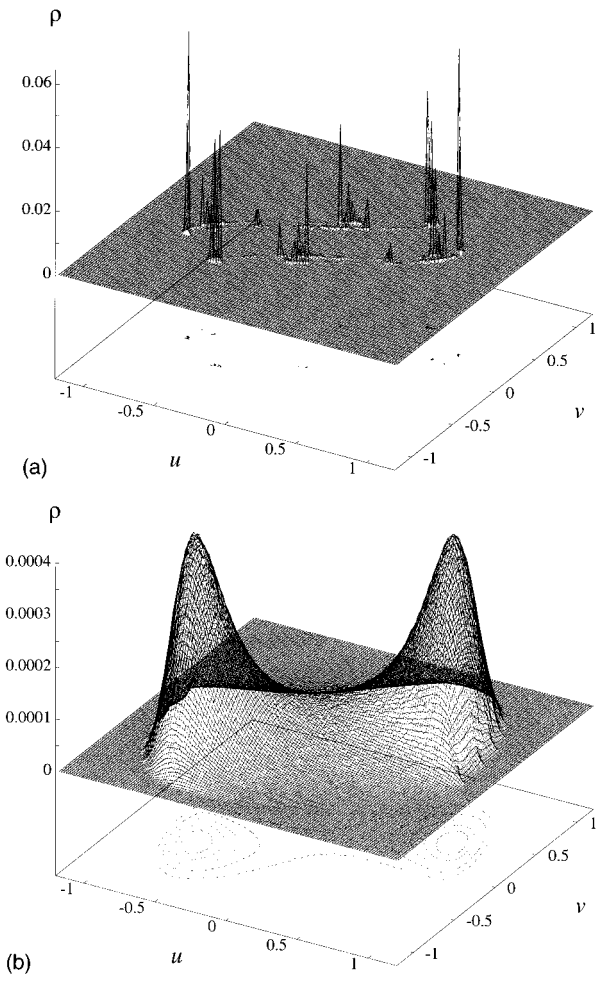

FIG. 7. Probability density $\rho(u,v)\times(2.56\times10^{-4})$ (on the 150×150 grid) at $\varepsilon=1.0$ for two values of the scale factor: (a) $\sigma=1$ and (b) $\sigma=4$.

the motion. Again, for small τ, the system behaves as if it were governed by the the averaged vector field subject to high-frequency noise. The noise has the effect of inducing transitions between the two stable fixed points (foci) of the averaged vector field. Since the transients resemble a relaxation oscillation, the resulting stochastic dynamics shows fast noisy jumps to the stable branches of the cubic nullcline. These then guide the stochastic flow to the vicinities of the stable foci. The repeated jumps and sojourns at the foci have periodic behavior. The attractors have the appearance of noisy limit cycles with density concentrated near the foci.

At large-τ values the attractor acquires structure near the foci and transverse to the fast segment of the oscillatory transient. Since τ is comparable to the time scale that characterizes the fast portion of the relaxation oscillation, one sees replication of folded motion near the foci and fast transients on the relaxation oscillation.

B. Approach to the white-noise limit

We have seen that the attractor structure depends on both τ and ε. In constructing Fig. 6 the amplitude Δ was held fixed. It is interesting to consider the approach to the white-noise limit starting with parameter values corresponding to particular attractors in Fig. 6 at small and large values of

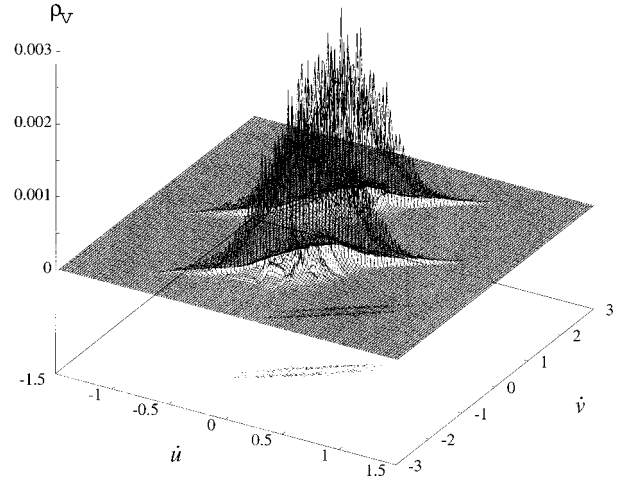

FIG. 8. Probability density $\rho_v(\dot{u},\dot{v})\times(8.0\times10^{-4})$ (on the 150×150 grid) at $\varepsilon=1.0$ at $\sigma=4$.

ε. As described earlier, this limit is approached as $\tau\to0$ and $\Delta\to\infty$ for $D=\Delta^2\tau$ fixed. To examine this structure we present results for the normalized coarse-grained invariant probability density $\rho(u,v)$ as a function of the phase-space variables (u,v).

First, consider $\varepsilon=1$, where the inhibitor is a fast variable, corresponding to the leftmost column of Fig. 6. Starting with the attractor at $\tau=2$, Δ is scaled by σ and τ by σ^{-2} so that D is fixed at $D=0.18$ and the white-noise limit is approached as $\sigma\to\infty$. In Fig. 7(a), for $(\varepsilon,\tau)=(1.0,2.0)$ at $\sigma=1$, $\rho(u,v)$ is quasifractal, while in Fig. 7(b) at $\sigma=4$, $\rho(u,v)$ is unstructured and bimodal, the density of a white-noise process having two stable fixed points. The change in ρ from (a) to (b) occurs through progressively smoother shapes as σ increases. Although the bimodal configuration-space density shown in Fig. 7(b) has a smooth form in the white-noise limit, there are correlations in velocity space due to the dichotomous nature of the noise process. These correlations can be seen in Fig. 8, where the probability density $\rho_v(\dot{u},\dot{v})$ in $(\dot{u},\dot{v})$ velocity space is shown. The noise process drives $\dot{v}$ and its dichotomous character shows itself the narrow double sail-like density in this figure. Each sail comprises two thin vanes. These sails have separation $O(\varepsilon\Delta)=O(\sigma)$ (ε fixed) $\sigma\to\infty$. However, $\dot{u}$ depends on the configuration variables u and v and since these are bounded, $\dot{u}$ is bounded; correspondingly, the projection of the two fragments of the density in Fig. 8 on the $\dot{u}$ density has a Gaussian shape that tends to a definite limit as $\sigma\to\infty$. The smooth behavior of u, v, and $\dot{u}$, combined with the divergent behavior of $\dot{v}$, is reminiscent of the Ornstein-Uhlenbeck process [11]. However, the dichotomous (as opposed to Gaussian) character of the driving noise process is always evident in ρ_v. That $\dot{v}$ but not $\dot{u}$ is noise driven is also seen in the sample paths of the stochastic differential equation (10) in (u,v) space where the fluctuations appear only in the v direction, indicating that noise is coupled to the velocity field $\dot{v}$.

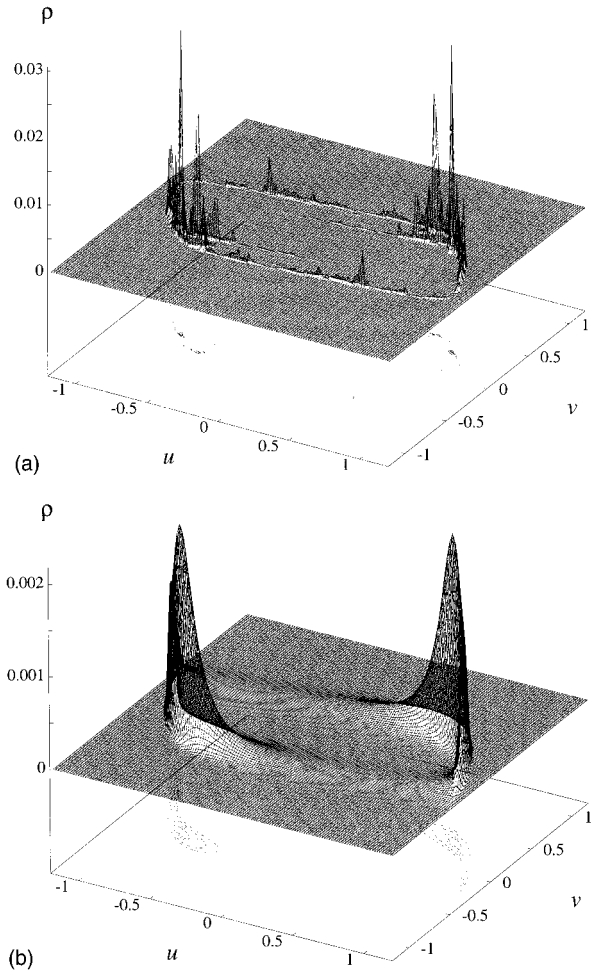

FIG. 9. Probability density $\rho(u,v)\times(2.56\times10^{-4})$ (on the 150×150 grid) at $\varepsilon=0.1$ for two values of the scale factor: (a) $\sigma=1$ and (b) $\sigma=4$.

An analogous change is seen in Fig. 9 in the slow-inhibitor regime at $\varepsilon=0.1$, the rightmost column of Fig. 6 where the attractor is a noise-driven limit cycle. Once again, one observes destruction of the attractor fine structure as the white-noise limit is approached, similar to that seen in the $\varepsilon=0.1$ column of Fig. 6 as τ decreases from top to bottom. Figure 9(a) ($\sigma=1$) shows a quasifractal limit-cycle density. The high-density regions near the two stable fixed points eject double jets; this density is structured along the direction of the stochastic flow, even in the fast relaxation part of the limit cycle. As σ increases the jets first replicate under the dichotomous noise process and then become smoothed by noise-induced diffusion. As σ increases further the structure in the density disappears steadily until, at $\sigma=4$ shown in Fig. 9(b), the density is smooth. For the reasons discussed previously the density ρ_v behaves like the density in Fig. 8.

V. TRANSITION PROCESSES

We now examine the transition processes related to the various kinds of attractor structure discussed above. For the parameter regime of interest here, the noisy attractors have high-density regions in (u,v) space in the vicinities of the two stable fixed points of the average vector field. However, the attractors are distinguished by the structure of the low-density regions that connect the high-density peaks. At small ε, the cubic nullcline controls the deterministic dynamics; in general the transient dynamics comprises fast motion towards a branch of the cubic nullcline followed by slow motion along this nullcline towards the stable fixed point. Under the influence of noise the system is excited into the phase-space regions corresponding to the transient dynamics so that the persistent motion resembles a noisy relaxation oscillation or limit cycle. In contrast, at large ε, the deterministic dynamics is controlled by the linear nullcline. In this case the noisy dynamics, which takes the system from one fixed-point region to the other, never excites the system far from this nullcline, so there is a single low-density band connecting the high-density regions.

It is helpful to give a qualitative description of the transient evolution from configurational δ-function initial states of these attractor types. These densities are $\delta(u-u_s)\delta(v-v_s)$, where (u_s,v_s) is the upper right stable fixed point of the averaged autonomous vector field.

Limit-cycle attractor structure, from the fractals that appear at large τ to the smooth configurational densities that appear as $\tau\to0$, at fixed $D=\Delta^2\tau$, are controlled by the cubic v nullcline. The successive distributions that evolve from the initial δ-function densities for the limit-cycle case show circulation and spreading. For values of τ that are comparable with the period t_{LC} associated with the noisy limit cycle, the density successively doubles under each application of the stochastic map. The circulation and duplication processes are mingled and atomic density appears at widely separated locations on the limit cycle in the first few map iterations. This discrete-time evolution continues until a distribution of mass resembling the invariant measure of the stochastic flow emerges. However, as τ decreases to values far smaller than t_{LC} the duplication of density and the associated spreading of the mass by random diffusive motion occurs more slowly than the advective transport of density round the limit cycle by the averaged autonomous vector field. Now drift and diffusion are distinguishable as the fast and slow phases of the relaxation oscillation associated with the limit cycle can be clearly seen.

For the bimodal densities and measures arising for large ε on the linear u nullcline very different transient behavior arises. The circulation is very largely suppressed, although vestiges of it appear in the correlation between position and transition flux near the linear nullcline. What is not apparent, however, is any massive circulation process of the configurational density.

In both kinds of motion described above the behavior of the transients clearly indicates the character of transition correlation and lifetime. A way of quantifying the small-ε (limit-cycle) and large-ε (diagonal) transitions is to follow the evolution of the species characteristic function defined as left or right (L or R) with respect to the line $u=0$ in the space of variable u. The characteristic functions are defined as follows: $\chi_L(u)$ for the species on the left of the origin is

$$\chi_{\mathrm{L}}(u)=\begin{cases}1 & \text{if } u<0\\ 0 & \text{if } u\geq0\end{cases} \tag{20}$$

and $\chi_R(u)=1-\chi_L(u)$ for species on the right of the origin.

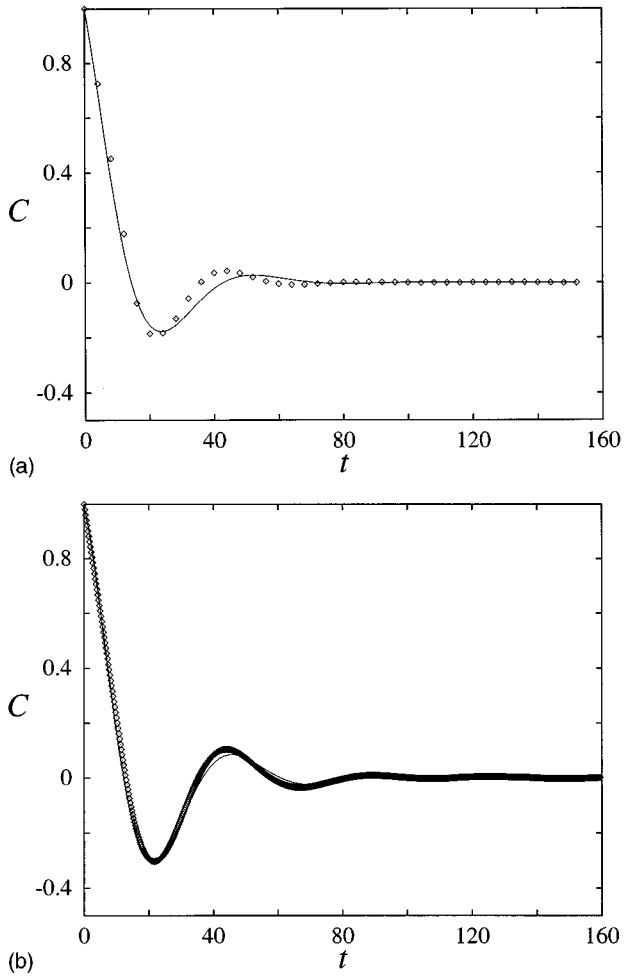

FIG. 10. Plots of $C(s\tau)=C_L(s\tau)$ vs $s\tau$ for the noisy limit-cycle case $\varepsilon=0.1$, corresponding to $D=0.36$. Panel (a) shows C_L for $\tau=4.00$ as diamonds; the continuous line is the best-fit exponential decay function $\exp(-0.0665t)\cos(0.1101t)$, where t is the continuous time. Panel (b) shows C_L for $\tau=0.25$ as diamonds; these nearly mask the best-fit decaying exponential function $\exp(-0.05218t)\cos(0.129t)$. This damped oscillatory decay is due to the circulation around the limit cycle, which has a period of $t_{\mathrm{LC}}\approx 50$ absolute time units as calculated from the cosine term. At $\tau=1.00$, C_L closely resembles that behavior shown in (b).

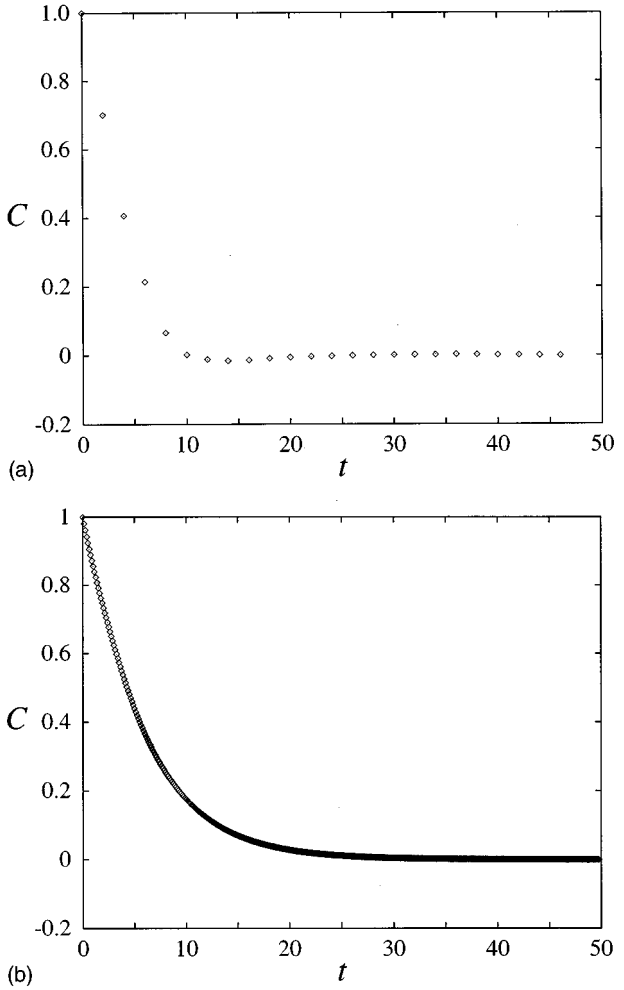

FIG. 11. Plots of $C(s\tau)=C_L(s\tau)$ vs $s\tau$ for $\varepsilon=1.00$ where transitions occur along the linear nullcline. The τ values corresponds to $D=0.18$. (a) $\tau=2.0$ and (b) $\tau=0.125$. As τ decreases the density of points on the t axis increases, but the exponential decay and decay lifetime are unaffected.

The χ_i $(i=L,R)$ generated by the map are time series (of binary variables), so that for a trajectory of duration T, i.e., $\{u(s):s=1,2,\ldots,T\}$, $C_i(s\tau)$, the normalized correlation functions with zero asymptotic mean, are estimated by the formula

$$C_i(s\tau)=\frac{\langle \delta\chi_i(s\tau)\,\delta\chi_i(0)\rangle_T}{\langle(\delta\chi_i)^2\rangle_T}, \tag{21}$$

where the time average is defined as $\langle A\rangle_T=\lim_{T\to\infty}(1/T)\Sigma_{s=0}^{T-1}A(s\tau)$ and $\delta\chi_i(s\tau)=\chi_i(s\tau)-\langle\chi_i\rangle_T$. To estimate these correlation functions, ensembles of random trajectories were generated with Bernoulli trial probabilities p and q.

The ensemble decay characteristics for the cubic (limit-cycle) and linear (diagonal) nullcline cases are now illustrated. Figure 10 shows a plot of the decay of $C_L(s\tau)$ vs $s\tau$ for parameters $\alpha=1.5$, $\varepsilon=0.1$, and $D=0.36$ corresponding to a noisy limit cycle. The decay is a strongly damped oscillation with the period of the limit cycle corresponding to the averaged vector field in the white-noise limit. Except for large $\tau=4.0$, the graphs are very similar, showing that processes with a time scale comparable to the limit cycle of period t_{LC}, such as the coherence-lifetime motion around the limit cycle, are unaffected by using $\tau\ll 4.0$. The value of D and the period t_{LC} itself determine these decay characteristics. Reducing the value of τ affects the structure of the sample path in velocity space, but not the gross features of the relaxation and decay in configuration space. Figure 11 shows nearly monotonic, exponential decay corresponding to motion along the linear nullcline at fixed diffusion constant value $D=0.18$. The decay of the autocorrelation function is very nearly independent of τ once it has become small enough, i.e., for $\tau<1.00$. Equivalently, the lifetime in either the L or R configurational state, the reciprocal of decay constant, is τ independent. This ensemble measure of transition rates is independent of τ for values of τ larger than those producing smoothness of the density $\rho(u,v)$, which occurs for $\tau\leqslant 0.2$ for the diagonal transitions but has a larger bound

$\tau < 1.0$ in the noisy limit-cycle regime. From Fig. 11(b) we see that only for the smallest-τ values do all vestiges of the oscillatory dynamics disappear. In this regime the correlation function decay satisfies the phenomenological law

$$C_L((s+1)\tau) = \lambda C_L(s\tau) \tag{22}$$

and the $\leftrightarrows$ transition process follows first-order kinetics with $\lambda = \exp[-(0.17 \pm 0.01)\tau]$. In the other regimes discussed above one observes a breakdown of the phenomenological law for first-order kinetics.

VI. DISCUSSION

The effect of additive periodic dichotomous noise on the FitzHugh-Nagumo equations, a nonpotential flow, has been examined as noise and system parameters are changed. The noise period τ, its amplitude Δ, and the stiffness parameter ε of the FHN equations have been varied to exhibit the phenomena described in this study.

The effects of these parameters can roughly be explained as follows. The behavior of the underlying autonomous planar system is controlled by the linear or cubic nullclines depending on whether ε is large or small. The period τ controls the contribution of the deterministic evolution, so that for τ large the map derived from the flow has structured or fractal orbits, whereas for τ small the high frequency of the noise destroys most of this structure. The noise amplitude Δ controls transition rates in the system. This classification depends on the following observations. The parameter $D = \Delta^2 \tau$ has the units of a diffusion constant; by keeping D fixed we find that transition rates in the system depend on D alone (at fixed ε), but the invariant coarse-grained density (attractor structure) depends on τ. Simple decay of the species autocorrelation function is consistent with structured densities. Formal white-noise limits of the noise process can be taken, viz., $\Delta \to \infty$ and $\tau \to 0$ at fixed D. Since noise drives only the v dynamical variable we find that phase-space, course-grained densities, dependent on the variables u, v, and $\dot{u}$ or some subset of these, look smooth and eventually converge in the white-noise limit, although $\dot{v}$ diverges linearly with Δ and the densities dependent on $\dot{v}$ always display dichotomous character. These limits are sometimes a delicate matter because of the ordering of the velocity relaxation time scales and the noise time scale τ. In general, a simple Fokker-Planck equation in the u variable can be derived. For example, the stationary density $\rho^*(u)$ in the u variable behaves like that of a Gaussian white-noise process in a one-dimensional quartic potential $V(u)$. Other one-dimensional limits in the u variable can be achieved when velocity relaxation in v is fast but τ is not small. In the fast-inhibitor limit the motion is restricted to the neighborhoods of the cubic nullcline and the projected density on u behaves like a one-dimensional stochastic map.

Noise will drive the system from simple deterministic behavior, e.g., relaxation to a focus, to noisy behavior resembling the deterministic behavior at nearby parameter values. Typically this promotes transitions in the system. At small ε, noise will excite the system into limit-cycle-like behavior when there is nearby limit cycle of the underlying system. When the noise is large enough the sojourn time of the representative points near the stable fixed points is short enough that the period of the limit cycle shows itself in the oscillatory decay of the species autocorrelation function. Coherence and periodicity have to be present to see this feature. We have not investigated the detailed dependence on the sojourn times, but when transitions rarely occur we would expect coherence to be lost. The oscillatory contribution appears even when the stationary density of the system is structured because the noise period τ that controls this structure is always shorter than the period of the limit cycle. When the underlying system is controlled by the linear nullcline at large ε, noise promotes transitions along the direction of this nullcline. Near the white-noise limit there is no obvious evidence of correlations between the positive or negative probability current and position. However, as the details in attractor structure appear with increasing τ, such correlations should be observed.

ACKNOWLEDGMENTS

This research was supported in part by grants from the Natural Sciences and Engineering Research Council of Canada.

APPENDIX

In this appendix we derive the one-variable Fokker-Planck equation (15) from the two-variable Perron-Frobenius equation (7). In order to carry out the reduction we need to examine the quantities $\exp(\mathcal{L}_\pm^\dagger \tau)\mathbf{y}$ that appear in the integral kernel in Eq. (7). Let τ_s be a short time interval that is assumed to be larger than the time that characterizes the fast evolution of the v variable, i.e., $\tau_s \varepsilon = \text{const} > 1$. We also suppose that $\tau_s/\tau \ll 1$.

In the limit $\tau_s \to 0$, $\varepsilon \to \infty$ with $\varepsilon \tau_s = \gamma$ with $\gamma = \text{const} > 1$ we may evaluate this propagator acting on $\mathbf{y}$ for the short time interval τ_s to obtain

$$e^{\mathcal{L}_\pm^\dagger \tau_s}\begin{pmatrix} u \\ v \end{pmatrix} = \begin{pmatrix} u \\ v - \alpha^{-1}(u - \alpha v \mp \Delta)(e^{-\gamma\alpha} - 1) \end{pmatrix}. \tag{A1}$$

This quantity enters in the argument of the δ function, so we may now compute the evolutions of the density for time τ_s under the $\mathcal{L}_\pm^\dagger$ operators. Thus

$$\begin{aligned} \rho_+(u,v,t+\tau_s) &= p \int du'\,dv'\,\delta(u - e^{\mathcal{L}_+^\dagger \tau_s} u')\,\delta(v - e^{\mathcal{L}_+^\dagger \tau_s} v') \\ &\quad \times \rho(u',v',t) = p \int du'\,dv'\,\delta(u - u') \\ &\quad \times \delta(v - v' + \alpha^{-1}(u' - \alpha v' - \Delta)(e^{-\gamma\alpha} - 1)) \\ &\quad \times \rho(u',v',t) = p e^{\gamma\alpha} \rho(u, \alpha^{-1}(u - \Delta) \\ &\quad + e^{\gamma\alpha}[v - \alpha^{-1}(u - \Delta)], t), \end{aligned} \tag{A2}$$

which may be written in the form

$$\begin{aligned} \rho_+(u, \alpha^{-1}(u-\Delta) + \xi_+, t+\tau_s) \\ = p e^{\gamma\alpha} \rho(u, \alpha^{-1}(u-\Delta) + e^{\gamma\alpha}\xi_+, t), \end{aligned} \tag{A3}$$

where $\xi_+ = v - \alpha^{-1}(u-\Delta)$. Now suppose we have a unit mass of probability fluid on a compact support surrounding the phase-space region of interest. Suppose $\xi_+ \neq 0$ and let $\gamma \to \infty$. This has two effects: the prefactor on the right-hand side diverges, indicating infinite compression of the density (as can be confirmed by integrating the appropriate equation of continuity with a singular velocity component in the v direction). Since $\xi_+ \neq 0$ the v coordinate of the density on the right-hand side tends to infinity and thus lies outside the support. It follows that the image density must be confined to the curve $v = \alpha^{-1}(u-\Delta)$. So after evolution through τ_s the density, which was originally defined on an area in phase space, collapses in a singular way onto a curve.

An exactly parallel argument can be applied to the evolution under $\mathcal{L}_-^\dagger$, but now we have

$$\rho_-(u, \alpha^{-1}(u+\Delta)+\xi_-, t+\tau_s) = q e^{\gamma\alpha} \rho(u, \alpha^{-1}(u+\Delta)+\xi_-, t), \tag{A4}$$

where $\xi_- = v - \alpha^{-1}(u+\Delta)$. Equations (A3) and (A4) can be summarized as

$$\rho_\pm(\mathbf{x}, t+\tau_s) \equiv \rho_\pm(\mathbf{x}, t+\tau_s)\,\delta(\xi_\pm) \equiv \rho_\pm(u, \alpha^{-1}(u \mp \Delta)+\xi_\pm, t+\tau_s), \tag{A5}$$

where, as before, $\xi_\pm = v - \alpha^{-1}(u \mp \Delta)$. The evolution from $t+\tau_s$ to $t+\tau$ occurs on the adiabatic curves implied by the δ-function constraints. The forward evolution, comprising the initial, short τ_s step and final, long $\tau - \tau_s$ step can now be written for ρ_+ as

$$\rho_+(\mathbf{x}, t+\tau) = p e^{\mathcal{L}_+ \tau} \rho(\mathbf{x}, t) = p e^{\mathcal{L}_+(\tau-\tau_s)} e^{\mathcal{L}_+ \tau_s} \rho(\mathbf{x}, t) = p e^{\mathcal{L}_+(\tau-\tau_s)} \rho_+(\mathbf{x}, t+\tau_s)\,\delta(\xi_+), \tag{A6}$$

where $\mathbf{x}$ implies that the density ρ_+ is supported on an area that after time τ_s collapses to a support on a one-dimensional manifold as explained previously. There is an analogous equation for ρ_-. Taking the sum of the $\rho_\pm$ contributions and expanding the evolution operator for the $\tau - \tau_s$ step to second order, we obtain, after division by $\tau - \tau_s$,

$$\frac{1}{\tau-\tau_s}(\rho(u,t+\tau) - \rho(u,t+\tau_s)) = \frac{1}{\tau-\tau_s}(\{1 - \mathcal{L}_+(\tau-\tau_s) + \tfrac{1}{2}[\mathcal{L}_+(\tau-\tau_s)]^2\}\rho_+(\mathbf{x}, t+\tau_s) + \{1 - \mathcal{L}_-(\tau-\tau_s) + \tfrac{1}{2}[\mathcal{L}_-(\tau-\tau_s)]^2\}\rho_-(\mathbf{x}, t+\tau_s) - \rho(\mathbf{x}, t+\tau_s)). \tag{A7}$$

In this equation the projected, summed density $\rho = \rho_+ + \rho_-$ on the left-hand side is written as a function of u only because the short-time (τ_s) evolution after each noise transition confines $\rho_\pm$ to the $\delta(\xi_\pm)$ adiabatic manifolds, i.e.,

$$\rho(u, t+\tau) \equiv \rho_+(\mathbf{x}, t+\tau)\,\delta(\xi_+) + \rho_-(\mathbf{x}, t+\tau)\,\delta(\xi_-). \tag{A8}$$

Substituting for $\mathcal{L}_\pm$ in Eq. (A7) and using $\mathcal{L}_\pm \rho_\pm(\mathbf{x}, \tau_s) \equiv \nabla \cdot \mathbf{f}_\pm \rho_\pm(\mathbf{x}, \tau_s)\,\delta(\xi_\pm)$ gives, in the limit $\tau - \tau_s \to 0$, for the formal time ordering $\tau \gg \tau_s \geqslant 0$, the Fokker-Planck equation (15) with diffusion coefficient $\widetilde{D} = D/\alpha^2$.

[1] The literature on this topic is extensive. For reviews see, for example, *Noise in Nonlinear Dynamical Systems*, edited by F. Moss and P. V. McClintock (Cambridge University Press, Cambridge, 1989), Vols. 1–3; P. Hänggi, P. Talkner, and M. Borkovec, Rev. Mod. Phys. **62**, 251 (1990).

[2] I. L'Heureux, R. Kapral, and K. Bar-Eli, J. Chem. Phys. **91**, 4285 (1989).

[3] K. Kitahara, W. Horsthemke, and R. Lefever, Phys. Lett. **70A**, 377 (1979).

[4] R. FitzHugh, Biophys. J. **1**, 445 (1961); J. Nagumo, S. Arimoto, and Y. Yoshikawa, Proc. IRE **50**, 2061 (1962).

[5] J. A. McFadden, IRE Trans. Inf. Theory **IT-5**, 174 (1959); A. R. Cohen, IRE Trans. Circuit Theory **CT-9**, 372 (1962).

[6] A. J. Irwin, S. J. Fraser, and R. Kapral, Phys. Rev. Lett. **64**, 2343 (1990); S. J. Fraser and R. Kapral, Phys. Rev. A **45**, 3412 (1992).

[7] The underlying stochastic process may also be a Markov chain. See, for instance, J. M. Porrà, J. Masoliver, and K. Lindenberg, Phys. Rev. E **48**, 951 (1994); J. M. Porrà and K. Lindenberg, *ibid.* **52**, 409 (1995).

[8] For the Bernoulli trials considered here the stochastic process acts on the total density at the instant of transition; however, for the Markov-chain case the transition matrix of the Markov chain acts on each density component.

[9] P. Erdös, Am. J. Math. **61**, 974 (1939); R. Salem, Duke Math. J. **11**, 103 (1944); *Algebraic Numbers and Fourier Analysis* (Wadsworth, Belmont, 1983).

[10] It is possible to follow the motion of such systems and examine their asymptotic behavior by replacing $\rho(\mathbf{y},t)d\mathbf{y}$ in Eq. (7) by some suitably defined, time-dependent measure $m(\mathbf{y},t)$ in which case Eq. (7) becomes a Stieltjes integral equation for the evolution of the measure.

[11] G. E. Uhlenbeck and L. S. Ornstein, Phys. Rev. **36**, 823 (1930).

[12] R. Kapral and S. J. Fraser, J. Stat. Phys. **70**, 61 (1993).